PREPRINT
M. Mirzaei, P. Ripka, V. Grim, A. Chirtsov: A Novel Position Sensor With a Conical Iron Core, IEEE Trans. Instrum. and meas. Vol. 69 , Iss 11, Nov. 2020, pp. 9178 - 9189 ,doi: 10.1109/TIM.2020.2999691

A Novel Position Sensor with Conical Iron Core

Mehran Mirzaei, Pavel Ripka and Vaclav Grim

Abstract— **A novel position sensor is presented in this paper for pneumatic and hydraulic cylinders applications. Solid iron core with conical shape surrounded by axisymmetric coils is an essential part of the proposed position sensor. Axisymmetric coils are used for excitation and voltage measurements. Annealing of conical solid iron core is also performed to homogenize magnetic properties and increase conical solid iron core permeability, which improves position sensor performance in terms of sensitivity and linearity. Analytical and finite element analyses are utilized along with measurements in order to analyze the performance of position sensor. The measurements of position sensors are performed for excitation coil inductance and pick up coils voltages. Different frequencies are considered for the analysis and measurements. The measurement results show the maximum linearity error is about 4% for the manufactured model and it is calculated maximum 1% for theoretical model.**

Index Terms—**Novel position sensor, conical iron core, annealing, eddy current, measurements, analytical and finite element analysis**

I. Introduction

THE contactless linear and angular position detecting of target objects is always a challenging issue [1]-[3].Piston position detecting in the pneumatic aluminum cylinder and hydraulic solid iron cylinder is a problematic work because it is shielded by conductive and magnetic covers [1]-[2]. Piston position in the cylinder is not symmetric and it is one side movement unlike LVDT position sensors [4], which moving armature budges in double sides.

Various internal and external sensors for pneumatic and hydraulic cylinders are implemented to detect positions of piston. Concerning pneumatic cylinder, internal sensors are inserted into the piston rod, which show mechanical complication and they are not cost effective and reliable. The microwave and optical sensors implemented inside the cylinder show same problems[5]-[8]. Permanent magnet on the piston in the external sensors can be used for aluminum cylinder, which has disadvantages. The necessity of using expensive non-magnetic stainless steel rod is the first disadvantage. The stainless non-magnetic steel must be

This work was supported in part by the Czech Technical University in Prague under Grant SGS18/187/OHK3/3T/1.
M. Mirzaei is with Faculty of Electrical Engineering, Czech Technical University, Prague 16627, Czech Republic (e-mail: mirzameh@fel.cvut.cz).
P. Ripka is with Faculty of Electrical Engineering, Czech Technical University, Prague 16627, Czech Republic (e-mail: ripka@fel.cvut.cz).
V. Grim is with Faculty of Electrical Engineering, Czech Technical University, Prague 16627, Czech Republic (e-mail: vaclav.grim@fel.cvut.cz).

used to cancel permanent magnet fields' distortion, which is caused by magnetic iron rod. Complicated mounting of permanent magnet on the piston is the second disadvantage. The temperature dependency of permanent magnets remanence flux density is another disadvantage, which is big weakness in the harsh environment.

The authors recently presented an AC-excited contactless piston position transducer with axial excitation and detection of radial magnetic field related to the end of magnetically soft iron rod [3].A moving ferromagnetic piston rod causes the magnetic field changes, which are sensed by an array of integrated fluxgate sensors mounted on the outside aluminum cylinder. The uncorrected maximum static error was ±3 mm with achievable 0.1 mm resolution. The dynamic performance is limiting factor for this sensor: the dynamic error is ±3 mm even at speed of 0.2 m/s. Complex signal processing of the sensor array is required for this type of sensor. Similar limitations were faced using radial excitation by saddle coils [9].

A simpler method is using variable inductance sensor, which was presented for hydraulic cylinder with non-metallic shell [10]. A modified inductance method as position sensor of a power cylinder with carbon steel shell was employed in [1] using differential coils configuration [11]. We have presented analysis and experimental results confirming that variable inductance sensors can also be utilized for detection of piston position in pneumatic cylinder with aluminum shell [12]. The inductance of the solenoid coils wound around aluminum cylinder changes with magnetic iron rod and piston position, which is affected by induced eddy current in the aluminum shell. Temperature stability of the variable inductance sensor for pneumatic cylinder was studied in [13]. The dynamic performance of variable inductance position sensor is problematic. Faster and more reliable solution especially for dynamic performance is to read and measure voltage, for example, pick up coil voltage of second coil wound around first layer of coil on the aluminum cylinder [14]. Measuring pick up voltage for position sensor is well known method for LVDT sensors with different cylindrical and flat type shapes configurations [15]-[18]. Alternative configuration to variable inductance sensor in [1], [10] and [12]-[14] is to implement coils around iron rod instead of cylinder however it is a cumbersome work because of long used coil for pneumatic and hydraulic cylinders [19]. Moving coils have problems with reliability is harsh environment.

In this paper, a novel position sensor with conical solid iron rod is presented, which has one excitation coil and two pick up coils with axisymmetric configurations. The inductance of excitation coil and induced voltage in the serially connected pick up coils are changing with conical iron rod displacement. The proposed position sensor has short length and small coils, which makes it appropriate and easy mountable in hydraulic and pneumatic cylinders. The inductance measurements are performed with a LCR meter and precise measurement of pick up coils voltage are done with a Lock in amplifier. 2D axisymmetric analytical and finite element analyses with eddy current solver are performed to evaluate the performance of position sensor with conical solid iron core at different frequencies along with measurements.

Compared to existing designs, our sensor has no moving coils, compact size and simple design.. Because of that it is very robust against external harsh environment. Unlike DC sensors based on magnet attached to the piston, which require expensive stainless-

steel piston rod material, the conical piston rod used in our sensor can be made of ordinary steel, which is cost effective.

II. Model of Position Sensor

A. Structure

3D model of the proposed position sensor with conical solid iron rod with axisymmetric configuration is shown in Fig. 1. One excitation coil and two serially connected pick up coils in the left and right sides of the excitation coil are used for the position sensor. Fig. 2(a) shows the 2D schematic side view for the position sensor with conical iron rod. The used iron is solid and the induced eddy current in the iron rod is considered in this paper. The full-scale moving range of the position sensor is 500 mm.

B. Dimensions and parameters

The dimensions and the parameters of the position sensor are presented in Table I according to Fig. 2 (a).

TABLE I

Dimensions and Parameters of Position Sensor

Parameter	Value
N_e	100
N_p	50
I_a	65.12 (mA)
L	700 (mm)
L_1	0 (mm)
L_2	40 (mm)
D_1	19.7 (mm)
D_2	30 (mm)
D_w	40 (mm)
l_e	10.4 (mm)
l_p	5.35 (mm)
d_w	1.75 (mm)
h_w	0.5 (mm)
σ_i	5.54 (MS/m)
$\mu_{r\text{-}i}$	115

where, N_e, N_p, I_a, σ_i and $\mu_{r\text{-}i}$ are number of turns in the excitation coil, number of turns in the pick up coil, rms value of current in the excitation coil, iron rod conductivity at room temperature and relative magnetic permeability of iron rod.

III. Performance Analysis of Position Sensor

An analytical method is used for the fast analysis and parametric calculations of position sensor with conical iron rod using simplified model in the Fig. 2 (b). The conical iron rod is replaced with equivalent cylindrical model in order to compute analytically the magnetic and electric parameters. The diameter D_m in Fig. 2 (b) is calculated equal to the conical iron rod diameter corresponding to the position of the middle point of excitation coil. The effective diameter, D_m in the analytical model of the equivalent cylindrical rod is adjusted for each position of coils. The self-inductance of excitation coil and pick-up coil voltage with air core and iron core in (A5) – (A6) are calculated using appendix A.

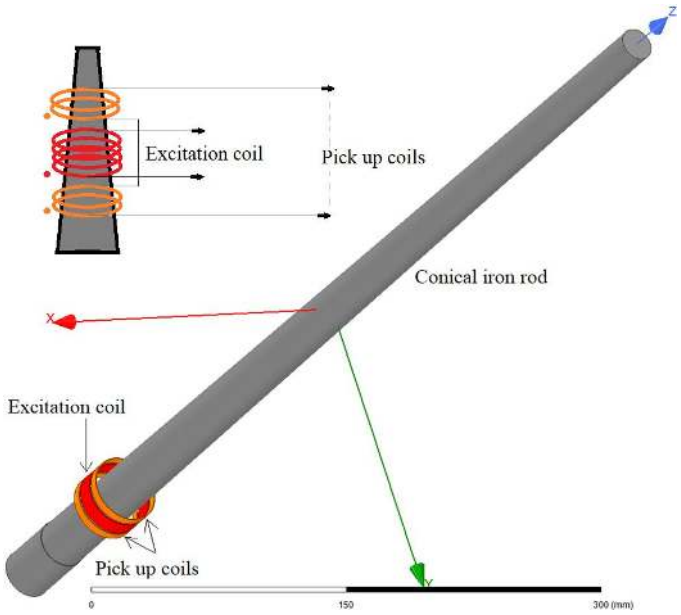

Fig. 1. 3D model of position sensor with conical iron rod with excitation coil and two serially connected pick up coils

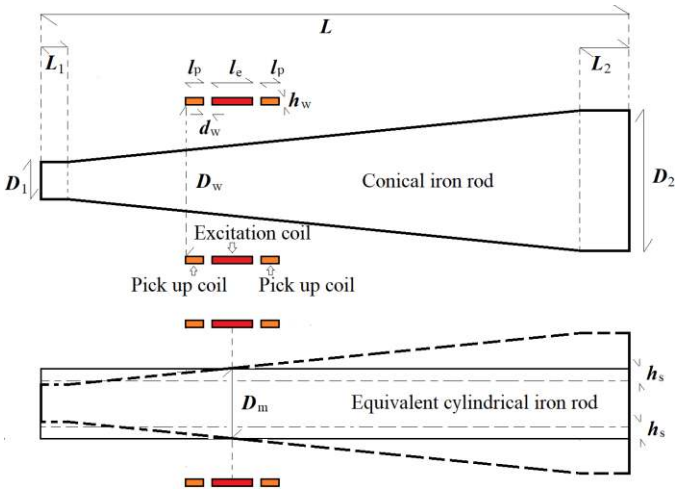

Fig. 2. Schematic model of side view of the position sensor with conical iron rod, (a) real conical model (up), (b) equivalent cylindrical model for conical iron rod (bottom)

The relative initial magnetic permeability is considered in this paper as magnetic fields of excitation coil are very small. *B-H* curve and relative magnetic permeability curve are presented in appendix C for iron rod material. The typical value, 115 is estimated for relative magnetic permeability of construction solid iron in Table I. The relative initial magnetic permeability of typical construction steels could be varied between 50 and 200 without annealing [20], which will be measured and analyzed in the next sections.

Firstly, the excitation coil inductance and pick up coils voltage are calculated and compared with measurements with air core and with cylindrical (non-conical) iron core in order to validate analytical formulas in (A5) - (A8). The comparison between analytical calculations and measurements results are presented in Table II and III, which shows high precision of analytical method. The length and diameter of cylindrical iron rod (non-conical) are 520 mm and 30 mm, respectively. The coils are located in the middle of iron rod axial length to avoid finite length effects.

Fig. 3 shows analytical calculations of excitation coil inductance and pick up coils voltages of position sensor with conical iron core (parameters and dimensions as Table I at 100 Hz, 200 Hz, 400 Hz and 1000 Hz. Excellent linearity is observed. The excitation coil inductance decreases with frequency due to the smaller skin and flux penetration depth in solid iron core and higher magnetic reluctance. The pick up coils voltage increases with frequency. The sensitivity of imaginary component of voltage is higher than real component of voltage. The zero position in the graphs corresponds to the point with 100 mm distance to the head of conical iron rod (smaller diameter, D_1 in Fig. 2). The imaginary (Im) and real (Re) components of the voltage are calculated based on the excitation coil current as a reference signal.

TABLE II

COMPARISON BETWEEN ANALYTICAL AND EXPERIMENTS WITH AIR CORE

Parameter	Exp./Ana.
$L_{s\text{-}air}$	577 (μH)/570(μH)
$U_{p\text{-}air}$– 100 Hz	10.71 (mV)/10.45(mV)

TABLE III

COMPARISON BETWEEN ANALYTICAL AND EXPERIMENTS WITH IRON CORE

Parameter	Experiment /Analytical (μ_r=115)
$L_{s\text{-}iron}$-20 Hz	2.28 (mH) / 2.25(mH)
$L_{s\text{-}iron}$-100 Hz	1.62 (mH)/ 1.66(mH)
$L_{s\text{-}iron}$-200 Hz	1.40 (mH) / 1.44(mH)
$L_{s\text{-}iron}$-400 Hz	1.22 (mH) / 1.26(mH)
$U_{p\text{-}iron}$– 1 Hz	0.25+i·1.14 (mV) / 0.04+i·1.09 (mV)
$U_{p\text{-}iron}$– 20 Hz	5.88+i·15.80 (mV) / 4.78+i·15.17 (mV)
$U_{p\text{-}iron}$– 100 Hz	23.11+i·52.02 (mV) / 20.04+i·51.66 (mV)
$U_{p\text{-}iron}$– 200 Hz	39.90+i·85.83 (mV) / 35.53+i·86.41 (mV)
$U_{p\text{-}iron}$– 400 Hz	67.56+i·141.12 (mV) / 61.93+i·143.58 (mV)

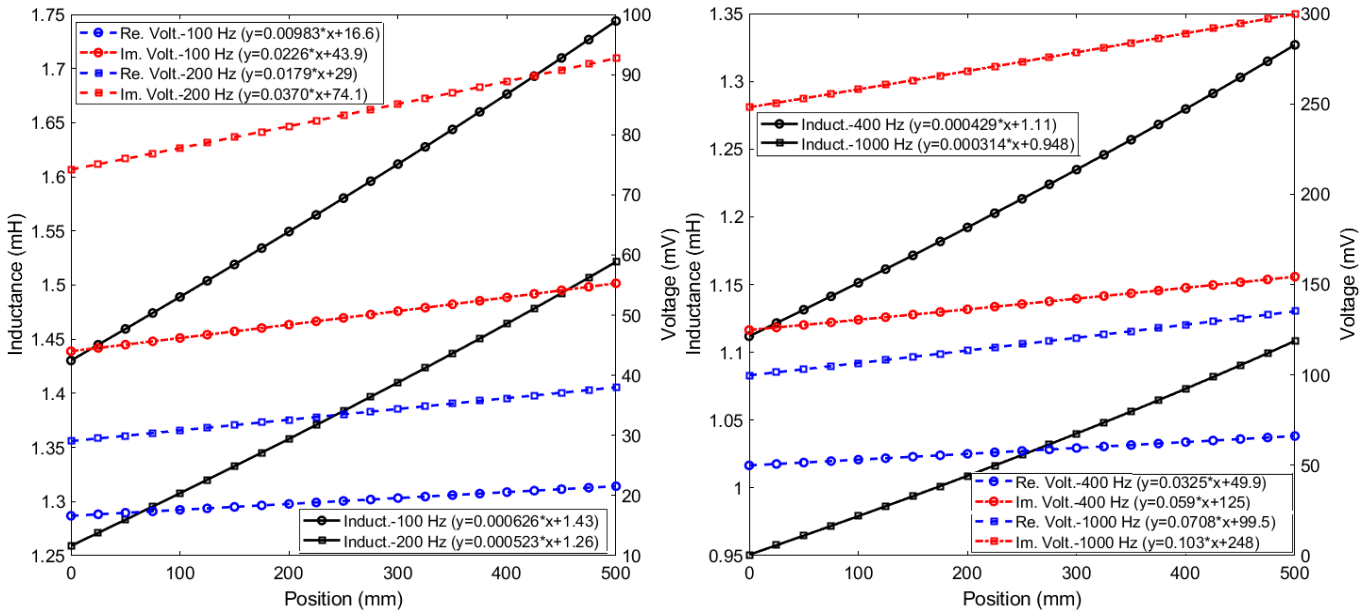

Fig. 3. Variation of excitation coil self-inductance and pick up coil voltage at 100 Hz, 200 Hz, 400 Hz and 1000 Hz(μ_r=150) - analytical

IV. EXPERIMENTS

Fig. 4 shows experimental setup and elements for position sensor with conical iron rod. Lock in amplifier (LIA) SR865 2 MHz DSP and LCR meter HP 4263B are used for the voltage and inductance measurements. Excitation coil is connected to signal generator Keithley 3390 50-MHz with internal resistance 50 Ω. The serially connected pick up coils are directly connected to input terminal IN-A of LIA without any interface. Terminal for reference signal of LIA is connected in parallel with small resistance, which is serially connected with excitation coil. Therefore, excitation coil current is reference signal and real and imaginary components of pick up coils voltage could be measured relative to the excitation coil current. The excitation and pick up coils electrically connected for grounding via LIA. The maximum output voltage of signal generator is selected 10 V (amplitude) to get maximum excitation current and maximum sensor output and sensitivity.

The conical iron rod was manufactured using machine tool from 700 mm axial length and 30 mm diameter cylindrical iron rod. The fabricated conical iron rod has not faultless smooth surface for conical part, which could affect linearity of the proposed position sensor.

A. Without Annealing

Fig. 5 shows magnetic flux distribution using 2D axisymmetric FEM [F] using time harmonic (eddy current) solver at different positions of coils relative to the conical iron rod. The ideal shape and surface are considered for the conical iron rod model in FEM simulations according to Table I. The simulations and measurements range is 500 mm from 100 mm of conical iron rod head to 600 mm as shown in Fig. 5.

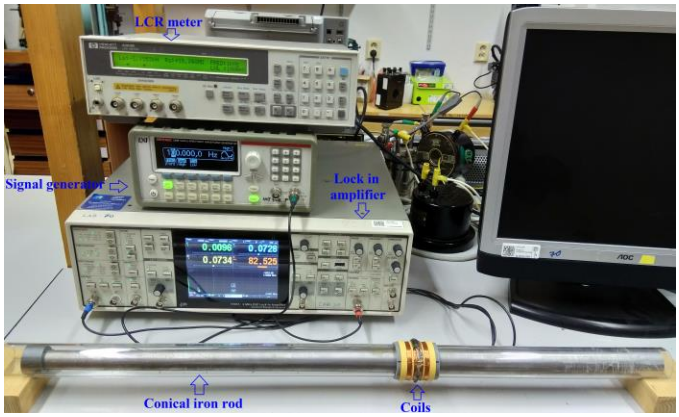

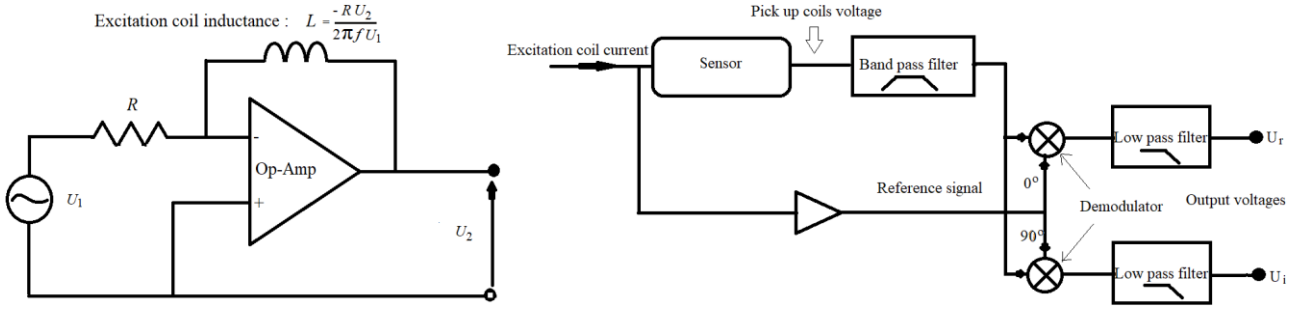

Fig. 4. Measurement elements for the position sensor, LCR meter, signal generator, lock in amplifier, coils and conical iron rod

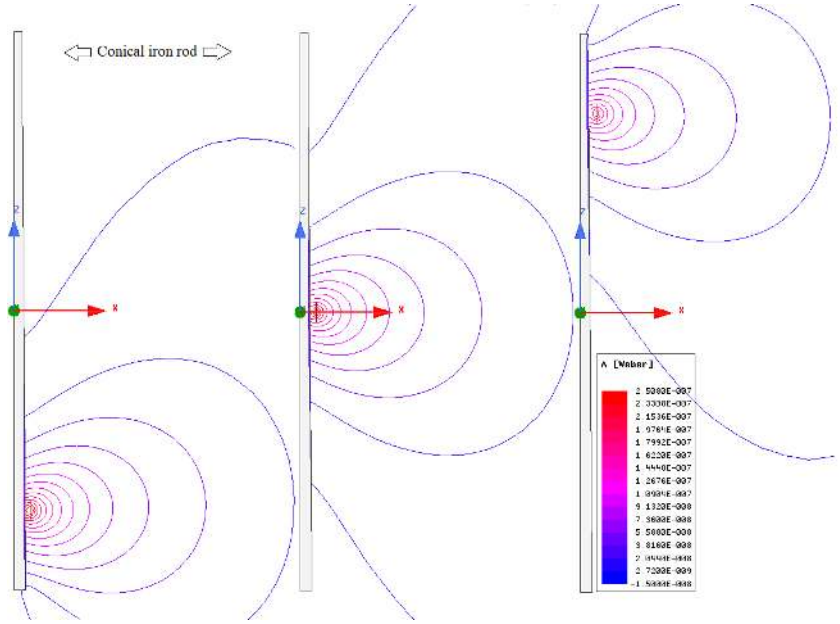

Fig. 5. Magnetic flux lines distribution at different positions of coils using FEM, (left) coils position at 500 mm (middle) coils position at 250 mm (right) coils position at 0 mm (f =100 Hz) – the total axial length of iron is 700 mm

The measured and simulated values of self-inductance and pick up voltage versus coils position are depicted in the Fig. 6 without annealing at 100 Hz and 400 Hz. The analytical results correspond very well with FEM, which shows negligible effects of the approximations used in the analytical method. The estimated relative magnetic permeability is about 125 using inductance measurement and it is estimated about 150 using measured pick up voltage. The excitation coil current is smaller for inductance measurement using LCR meter in comparison to the current for pick up coils voltage measurement using lock in amplifier. Therefore produced magnetic field is lower in the iron rod for inductance measurements because of lower current.

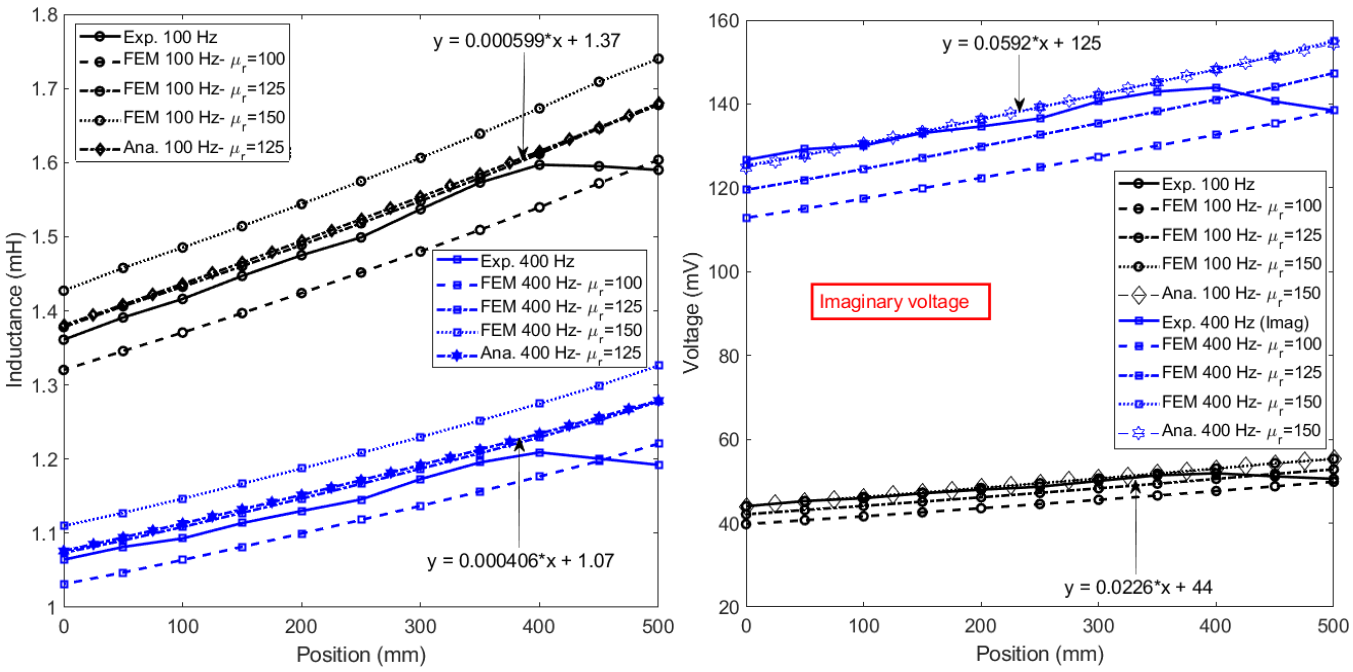

Fig. 6. Variation of excitation coil self-inductance and pick up coil voltage at 100 Hz and 400 Hz – non-annealed

The magnetic permeability is higher at high current or equivalent magnetic field strength in the iron rod as the operating point is in Rayleigh region of *B-H* curve.

The inductances and pick up voltages monotonically increase until position 400 mm and then they decrease until position 500 mm, which is not expected in the FEM and analytical calculations. The first reason is non smooth conical surfacenear end position, 500 mm because of machining. Second reason is presumed to be non-homogenized magnetic permeability distribution again because of machining, which could be minimized with proper annealing [21]. Non-straight measured curves and their fluctuations in whole measured positions range in comparison with straight curve of simulated values could be also improved by annealing and removing saliency parts in conical surface with more precise machining or casting.

B. With Annealing

Relaxation and homogenization annealing process is performed in order to improve magnetic properties of conical iron rod.The rod was annealed in vacuum, 2 hours at 800 deg C, slowly (8 hours) cooled down to 500 C, fast cooled (1h) to room temperature (appendix B). In order to evaluate the annealing effect, firstly two small samples (annealed and non-annealed) with axial length 70 mm and diameter 30 mm from same material as conical iron rod are used for measurements and simulations as shown in Fig. 7.

TABLE IV

COMPARISON BETWEEN ANALYTICAL AND EXPERIMENTS WITH IRON CORE-NON-ANNEALED

Parameter	Experiment / FEM (μ_r=115)
$L_{s\text{-}iron}$-20 Hz	1.61 (mH) / 1.62 (mH)
$L_{s\text{-}iron}$-100 Hz	1.44 (mH) / 1.47(mH)
$L_{s\text{-}iron}$-200 Hz	1.33 (mH) / 1.37 (mH)
$L_{s\text{-}iron}$-400 Hz	1.21 (mH) / 1.25 (mH)
$U_{p\text{-}iron}$– 1 Hz	0.09+i·0.51 (mV) / 0.01+i·0.52 (mV)
$U_{p\text{-}iron}$– 20 Hz	1.0+i·9.87 (mV) / 0.85+i·9.86 (mV)
$U_{p\text{-}iron}$– 100 Hz	8.57+i·43.22 (mV) / 7.51 +i·43.41 (mV)
$U_{p\text{-}iron}$– 200 Hz	19.92+i·77.88 (mV) / 17.72+i·79.21 (mV)
$U_{p\text{-}iron}$– 400 Hz	42.4+i·136.1 (mV) / 39.41+i·140.4 (mV)

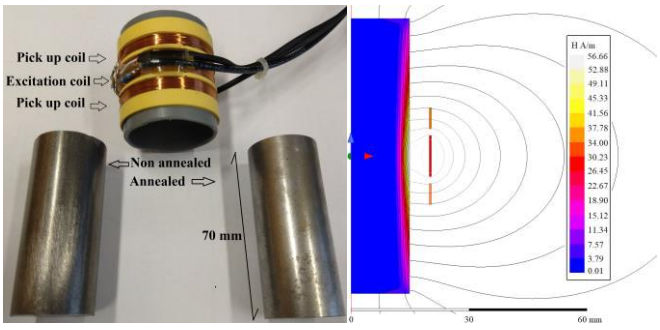

Fig. 7. Annealed and non-annealed iron rods with 70 mm length (left) and magnetic flux distribution and magnetic field strength at f= 100 Hz with μ_i=115 (right)

TABLE V

COMPARISON BETWEEN ANALYTICAL AND EXPERIMENTS WITH IRON CORE-ANNEALED

Parameter	Experiment / FEM (μ_i=400)
$L_{s\text{-}iron}$-20 Hz	1.70 (mH) / 1.70 (mH)
$L_{s\text{-}iron}$-100 Hz	1.61 (mH) / 1.61(mH)
$L_{s\text{-}iron}$-200 Hz	1.53 (mH) / 1.54 (mH)
$L_{s\text{-}iron}$-400 Hz	1.44 (mH) / 1.46(mH)
$U_{p\text{-}iron}$– 1 Hz	0.09+i·0.55 (mV) / 0.01+i·0.54 (mV)
$U_{p\text{-}iron}$– 20 Hz	0.68+i·10.60 (mV) / 0.53+i·10.46 (mV)
$U_{p\text{-}iron}$– 100 Hz	5.63+i·49.80 (mV) / 5.13+i·48.75 (mV)
$U_{p\text{-}iron}$– 200 Hz	13.80+i·95.02 (mV) / 13.05+i·92.52 (mV)
$U_{p\text{-}iron}$– 400 Hz	32.60+i·178.65 (mV) / 31.89+i·172.05 (mV)

Tables IV and V present comparison of measurements results with and without annealing. The estimated relative magnetic permeability is increased 3.5 (400/115) times in annealed sample relative to non-annealed sample. The maximum changing of results because of annealing is occurred at 400 Hz, which is about 20%.

Monotonically increasing of measured inductances and voltages continues until 450 mm in annealed conical iron rod (Fig. 8), which shows larger linear range and values closer to the simulations results. It can be convinced that break point in measurement curves at 450 mm is caused by imperfect machining of conical surface. The annealing causes to increase sensitivity of the position sensor between 25% in inductance values at 100 Hz and 45% in voltage values at 400 Hz due to the higher magnetic permeability.

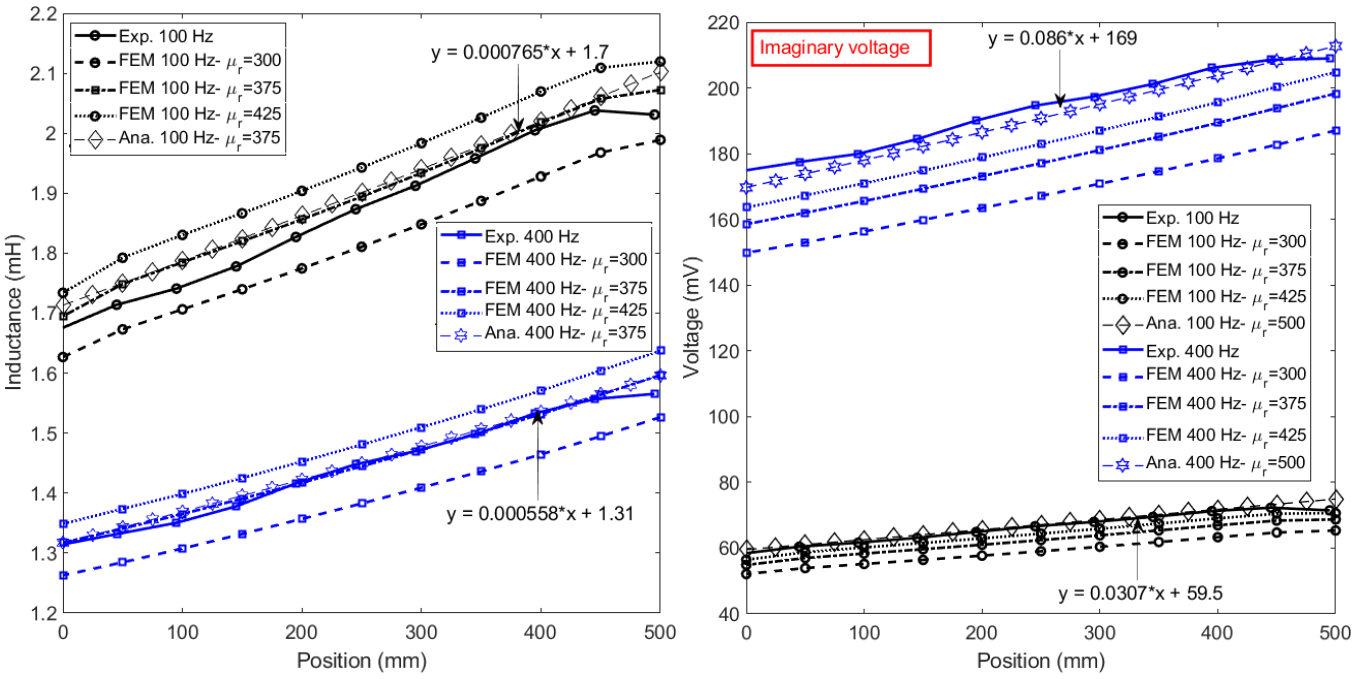

Fig. 8. Variation of excitation coil self-inductance and pick up coil voltage at 100 Hz and 400 Hz –annealed

Simulated voltages and inductances (Fig. 8) after annealing of conical iron rod at 100 Hz is less linear especially after start point and before end point in the annealed iron core, which could be caused by effect of increased relative magnetic permeability.

The magnetic yoke around coils using thin permalloy tape or silicon steel lamination helps to increase sensitivity of the position sensor and shield it against external magnetic fields. It will be investigated in the future works to evaluate increasing sensitivity and improving linearity.

V. Linearity Analysis

The piston stroke and realistic moving range of piston is typically shorter than the cylinder length for real pneumatic cylinders [14]. Therefore, the linearity analysis is performed between 50 mm to 450 mm. The moving range of piston is practically 400 mm in this paper. The linear curve function between relative position of coils and conical iron rod, X(mm) versus inductance or voltage, Y (mH or mV) is presented as follows:

$$X = C \cdot Y + X_0 \tag{5}$$

Table VI presents values of parameters in (5). The linearity error is calculated from linear curve function values, X_l in (5) and experimental values, X_m for 400 mm stroke using as follows:

$$Error\ (\%) = (X_l - X_m\ )/400 \cdot 100$$

(6)

TABLE VI

LINEAR CURVE FUNCTION BETWEEN RELATIVE POSITION OF COILS AND CONICAL IRON ROD, *X* VERSUS MEASURED INDUCTANCE OR VOLTAGE, *Y*

Curves	$X=C\cdot Y+X_0$
$L_{s\text{-}iron}$-100 Hz	1181·Y-1966
$L_{s\text{-}iron}$-200 Hz	1411·Y-2072
$L_{s\text{-}iron}$-400 Hz	1717·Y-2232
$L_{s\text{-}iron}$-1000 Hz	2249·Y-2498
$U_{p\text{-}iron}$– 100 Hz	32.56·Y-1918
$U_{p\text{-}iron}$– 400 Hz	12.24·Y-2121

The error calculations are shown in Fig. 9, which has maximum values about 4% for experimental results. Overall linearity using measured inductance at 200 Hz (Fig. 10) is the finest results. The error results for analytical calculations show maximum error 1% for 400 mm stroke, which can be achievable for precisely machined rod. It should be noted that these results were obtained without any corrections.

The linearity errors using analytical model increase at extreme positions of 25 mm and 475 mm, which is because of finite length effects (end effects) of conical iron rod. First suggestion is increasing axial length of conical iron rod to decrease errors of finite length effects. Second suggestion is optimization of coils dimensions and conical surface in order to minimize linearity error caused by finite length of iron rod, which is beyond this paper scope.

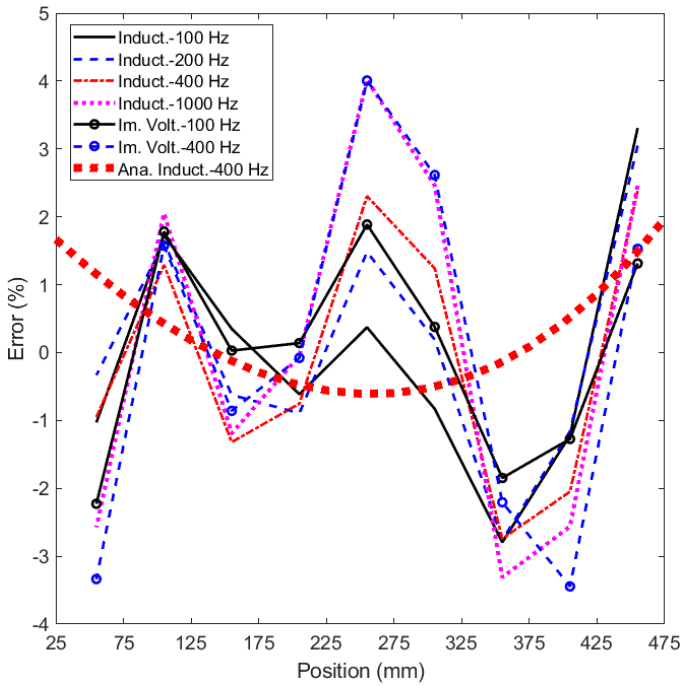

Fig. 9. Error calculations for 400 mm stroke based on the inductance and voltage values– using annealed conical iron rod

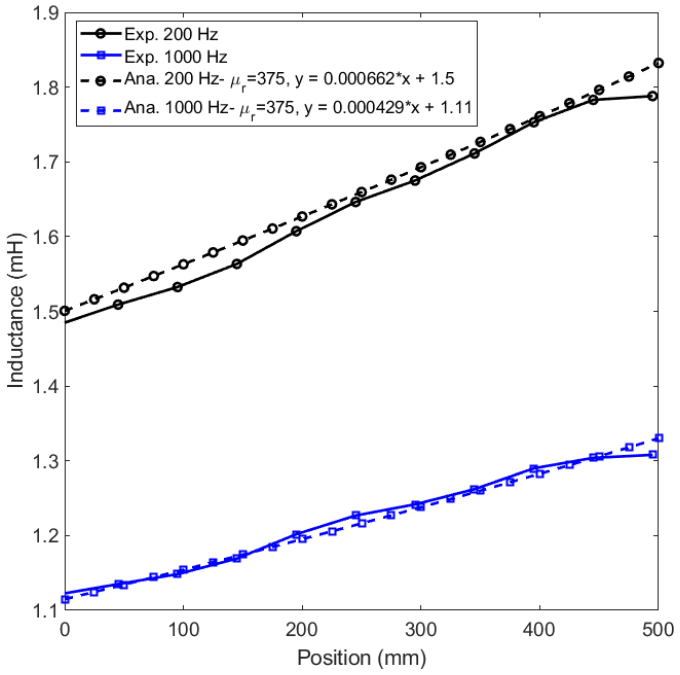

Fig. 10. Variation of excitation coil self-inductance at 200 Hz and 1000 Hz –annealed

Conical iron rod diameters have been measured in each 1 cm distance for precise modeling of the real surface of manufactured conical iron rod in FEM environment. FEM results comparison between more precise model of manufactured conical iron surface and smooth (perfect) of conical iron rod is shown in Fig. 11. It confirms that some nonlinearities in the measurements results are caused by non-uniform and non-smooth surface of the manufactured conical iron rod.

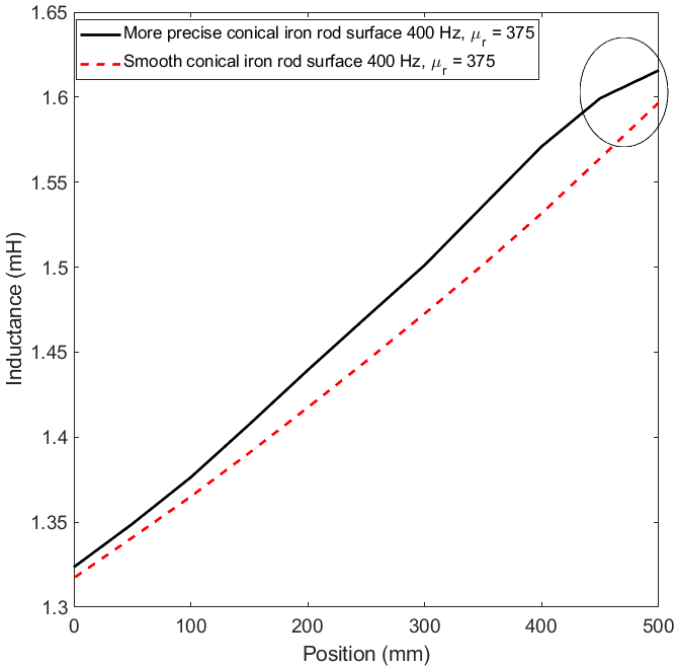

Fig. 11. Comparison between FEM results for smooth ideal surface and more precise surface modeling of manufactured conical iron rod

VI. Discussions

A potential method to compensate the temperature, the materials effects of solid iron rod and eccentricity changing could be multi-frequency sensor technique and pulsed eddy current method [22]-[23], which will be investigated in the future works. The iron rod temperature changes electrical conductivity and magnetic permeability, which affect reluctance of magnetic flux path and magnetic flux penetration depth, h_s (Fig. 2 b) and skin effect depth, δ.

Non-uniformity depth on the surface of conical iron rod strongly affects measurement accuracy in terms of fluctuations of results if it is larger than skin depth [4]:

$$\delta = \sqrt{\frac{2}{\omega\mu\sigma_i}}, \omega = 2\pi f \quad (7)$$

where, μ, σ_i and f are magnetic permeability and electrical conductivity and frequency, respectively. In addition to make conical surface as perfect as possible to avoid fluctuations of the results, using artificial neural networks could help to improve linearity by about one order of magnitude [18].

Recent works for alternative configurations of position sensors for pneumatic cylinders and hydraulic cylinders using ironless inductive position sensor [24] and variable reluctance differential solenoid transducer [25] are not applicable for pneumatic cylinders and hydraulic cylinders with large operating position range.

The developed analytical method despite its simplicity has almost same accuracy as 2D FEM because the effects of finite length of the iron rod is negligible at frequencies above 400 Hz even with high relative magnetic permeability about 400-500. Analytical methods are always preferable to numerical calculations [26] if its accuracy is in satisfactory range [23].

Measuring voltage is more dynamic, preferable and suitable for position measurement relative to inductance measurement. Two serially connected pick up coils in left and right sides of excitation coil is preferred to one pick up in one side of excitation coil to avoid end effects (finite axial length effect of conical iron) by vectorial summation or averaging of voltages of two pick up coils. Pick up voltage can be on top of excitation coil if excitation coil inductance is desired for position measurement, which induced voltage will be proportional to excitation coil inductance because of high coupling between excitation coil and pick up coils. Using fast rms measurements of voltages is not recommended as rms or absolute value is vectorial summation of real and imaginary components of voltage, which will be less linear in comparison with linearity of individual real and imaginary components. The

main drawback of measuring real or imaginary component could be less dynamic performance of sensor because of more time consuming signal processing, however it is more tolerant to the noise in comparison with simple rms reading.

First possible limitation of the proposed position sensor is operating in variable temperature environments without temperature compensation as temperature changes magnetic permeability and conductivity and sensor performance. Second possible limitation is requirement of complicated mechanical structure to provide smooth movement of conical iron rod and piston.

VII. Conclusion

Experimental results and theoretical calculations were presented for the position sensor with conical solid iron core. The proposed position sensor shows promising performance despite its simplicity. The main purpose of presented position sensor is for detecting of piston position in pneumatic cylinders and hydraulic cylinders however it could be operated for wide varieties of industrial applications. 2D axisymmetric analytical method and 2D axisymmetric FEM were used to evaluate and analyze position sensor performance. Analytical method is preferred at the design and optimization stages in comparison with 2D FEM as the parametric analysis of the position sensor is easier and faster. Operation of position sensor at high frequencies, 400 Hz and above is preferable as dynamic performance is better.

High precision of large range position measurement is possible with conical iron rod configuration without using long excitation coil and pick up coils. The linearity of presented results can be improved using smoother conical surface of iron rod as the angle of conical surface slope must be constant in whole range of conical part. Maximum linearity error was shown 4% for measurement results of manufactured model and it was maximum 1% for theoretical model. The optimization of the conical iron rod and size and positions of coils could improve more linearity and decrease linearity error considerable below 1%, which will be investigated in the future works. The effect of iron rod materials must be considered and compensated as construction steels and irons have different initial permeability and electrical conductivity.

It was shown that the proper annealing of the iron rod has high constructive impact on the position sensor performance in terms of increasing sensitivity and linearity as magnetic permeability is increased and homogenized especially in the machined conical surface.

Precise manufacturing of conical iron rod to have faultless conical surface, optimization of coils dimensions and relative positions of them, calculating optimum axial length of conical iron and using magnetic yoke and shielding are planned to increase sensitivity and improving linearity for future works. Dynamic analysis of sensor performance at transient conditions and thermal stability evaluation is also required to present the proposed sensor for industrial applications.

Appendix A: Analytical Equations

The sketch of conical iron rod is transformed to an equivalent cylindrical rod with diameter D_m (Fig. 2). The diameter, D_m is

calculated equal to the conical iron rod diameter corresponding to the middle point position of coils as shown in Fig. 2.

Governing differential equations versus magnetic vector potential for three regions ($A_{\phi,1}$ for air part beyond coils in region 1, $A_{\phi,2}$ for region 2 in air part between iron rod and coil and $A_{\phi,3}$ for iron rod in region 3) in computational model of Fig. A1 are extracted from Maxwell equations in the cylindrical coordinates [26] – [27]. The coils area regions are transformed to the line regions to simplify the computational model as coils radial thickness is just 0.5 mm (Fig. A1). Only azimuthal component of magnetic vector potential, A_ϕ is considered because of axisymmetric structure:

$$1/r\,\partial/\partial r\left(r\,\partial A_{\phi,1}/\partial r\right)+\partial^2 A_{\phi,1}/\partial z^2-A_{\phi,1}/r^2=0$$

$$1/r\,\partial/\partial r\left(r\,\partial A_{\phi,2}/\partial r\right)+\partial^2 A_{\phi,2}/\partial z^2-A_{\phi,2}/r^2=0$$

$$1/r\,\partial/\partial r\left(r\,\partial A_{\phi,3}/\partial r\right)+\partial^2 A_{\phi,3}/\partial z^2-A_{\phi,3}/r^2=\sigma_i\cdot\mu_3\cdot\partial A_{\phi,3}/\partial t$$

(A1)

The method of separation of variables (method of Fourier) is used to solve (A1) [26]-[27]:

$$A_{\phi,1}=\sum_{n=\pm1,\pm3,\cdots}\left(C_{11}I_1(m\cdot r)+C_{12}K_1(m\cdot r)\right)\cdot e^{j(\omega t-mz)}$$

$$A_{\phi,2}=\sum_{n=\pm1,\pm3,\cdots}\left(C_{21}I_1(m\cdot r)+C_{22}K_1(m\cdot r)\right)\cdot e^{j(\omega t-mz)}$$

$$A_{\phi,3}=\sum_{n=\pm1,\pm3,\cdots}\left(C_{31}J_1(\gamma\cdot r)+C_{32}Y_1(\gamma\cdot r)\right)\cdot e^{j(\omega t-mz)}$$

$$m=\left|\frac{n\pi}{L}\right|,\gamma=\sqrt{-m^2-j\omega\mu_3\sigma_i}$$

(A2)

where I_1, J_1, K_1 and Y_1 are Bessel functions with order 1 [N]. n is space harmonic order. L is axial length of iron rod. C_{11}, C_{12}, C_{21}, C_{22}, C_{31} and C_{32} are constants, which are obtained by the following boundary conditions:

$$A_{\phi,1}\left(\frac{D_m}{2}\right)=A_{\phi,2}\left(\frac{D_m}{2}\right),\qquad A_{\phi,2}\left(\frac{D'_w}{2}\right)=A_{\phi,3}\left(\frac{D'_w}{2}\right)$$

$$H_{z,1}\left(\frac{D_m}{2}\right)=H_{z,2}\left(\frac{D_m}{2}\right),\qquad H_{z,2}\left(\frac{D'_w}{2}\right)-H_{z,3}\left(\frac{D'_w}{2}\right)=J_s$$

$$D'_w=D_w+h_w$$

$$J_s = \sum_{n=\pm1,\pm3,\cdots} J_{sn} \cdot e^{j(\omega t - mz)}, \qquad J_{sn} = \frac{2}{n\pi} sin\left(m\frac{l_e}{2}\right) \cdot \frac{N_e \cdot I_a}{l_e}$$

$$H_z = 1/r\,\partial/\partial r\left(rA_\phi\right)/\mu$$

(A3)

where, H_z is magnetic field strength.

The self-inductance of excitation coil, L_s and pick-up coil voltage, U_p are calculated using following equations:

$$L_s = \frac{\Psi}{I_a} = \frac{N_e \cdot \int A_\phi ds}{I_a \cdot l_e},\ U_p = -j\omega\Psi = -j\omega\frac{N_p \cdot \int A_\phi ds}{l_p}, \qquad ds = rd\phi dz = 2\pi r dz = \pi D'_w dz$$

(A4)

The parameter A_ϕ is magnetic vector potential on the boundary between regions 2 and 3. We used $A_{\phi,3}$ in (A2) for integration in (A4). The integral in (A4) is performed on the boundary between regions 2 and 3, where surface regions of coils are simplified as line region between regions 2 and 3 in Fig. A1 in 2D view and they are cylindrical surfaces as shown in Fig. A1. The integration in (A4) is performed on the cylindrical surface of the coils. The integrations for voltage of two pick up coils are summed as they are serially connected.

The self inductance of excitation coil with air core, $L_{s\text{-}air}$ and with iron core, $L_{s\text{-}core}$ and pick up coil voltage with air core, $U_{p\text{-}air}$ and with iron core $U_{p\text{-}core}$ are calculated in (A5) – (A8) using (A4).

$$L_{s-air} = \sum_{n=\pm1,\pm3,\cdots} C_a \frac{2\pi \cdot D'_w}{m \cdot I_a \cdot l_e} N_e \cdot \sin\left(\frac{m \cdot l_e}{2}\right), C_a$$

$$= \frac{\mu_0 \cdot J_{sn}}{m \cdot C'_a}, C'_a = \left(I_0\left(m\frac{D'_w}{2}\right)/I_1\left(m\frac{D'_w}{2}\right) + K_0\left(m\frac{D'_w}{2}\right)/K_1\left(m\frac{D'_w}{2}\right)\right)$$

(A5)

$$U_{p-air} = j\omega \cdot \sum_{n=\pm1,\pm3,\cdots} C_a \frac{4\pi \cdot D'_w}{m \cdot l_p} N_p \cdot \sin\left(\frac{m \cdot l_p}{2}\right) \cdot \cos\left(\frac{m \cdot \left(l_e + l_p + 2d_w\right)}{2}\right)$$

(A6)

$$L_{s-iron} = \sum_{n=\pm1,\pm3,\cdots} C_i \frac{2\pi \cdot D'_w}{m \cdot I_a \cdot l_e} N_e \cdot \sin\left(\frac{m \cdot l_e}{2}\right), C_i$$

$$= \frac{\mu_0 \cdot J_{sn}}{m \cdot C'_i}, C'_i$$

$$= \left(I_0\left(m\frac{D'_w}{2}\right) \cdot C''_{i-12} - K_0\left(m\frac{D'_w}{2}\right)\right)$$

$$/\left(I_1\left(m\frac{D'_w}{2}\right) \cdot C''_{i-12} + K_1\left(m\frac{D'_w}{2}\right)\right) + K_0\left(m\frac{D'_w}{2}\right)/K_1\left(m\frac{D'_w}{2}\right), C''_{i-12} = C''_{i-1}/C''_{i-2}, C''_{i-1}$$

$$= m \cdot K_0\left(m\frac{D_m}{2}\right) \cdot J_1\left(\lambda\frac{D_m}{2}\right) + \frac{\lambda}{\mu_{r-i}} \cdot K_1\left(m\frac{D_m}{2}\right)$$

$$\cdot J_0\left(\lambda\frac{D_m}{2}\right), C''_{i-2} = m \cdot I_0\left(m\frac{D_m}{2}\right) \cdot J_1\left(\lambda\frac{D_m}{2}\right)$$

$$-\frac{\lambda}{\mu_{r-i}} \cdot I_1\left(m\frac{D_m}{2}\right) \cdot J_0\left(\lambda\frac{D_m}{2}\right)$$

(A7)

$$U_{p-iron} = j\omega \cdot \sum_{n=\pm1,\pm3,\cdots} C_i \frac{4\pi \cdot D'_w}{m \cdot l_p} N_p \cdot \sin\left(\frac{m \cdot l_p}{2}\right) \cdot \cos\left(\frac{m \cdot \left(l_e + l_p + 2d_w\right)}{2}\right)$$

(A8)

where I_0, J_0 and K_0 are Bessel functions with order of 0 [N].

Fig. A2 shows magnetic flux distribution calculated using analytical method for different equivalent iron rod radiuses, which correspond to different relative positions of coils to the conical iron rod.

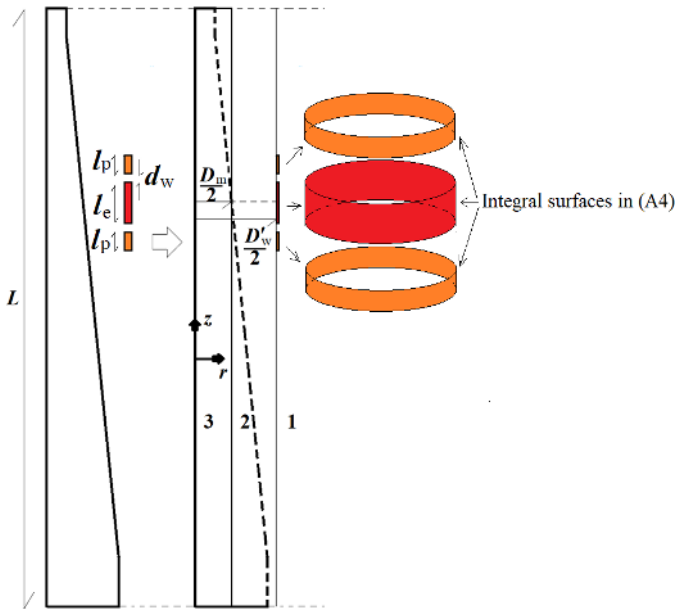

Fig. A1. Computational 2D axisymmetric model for position sensor with conical iron rod – transformation of real shape of conical iron rod to the cylindrical iron rod with equivalent diameter, D_m , which changes with coils position

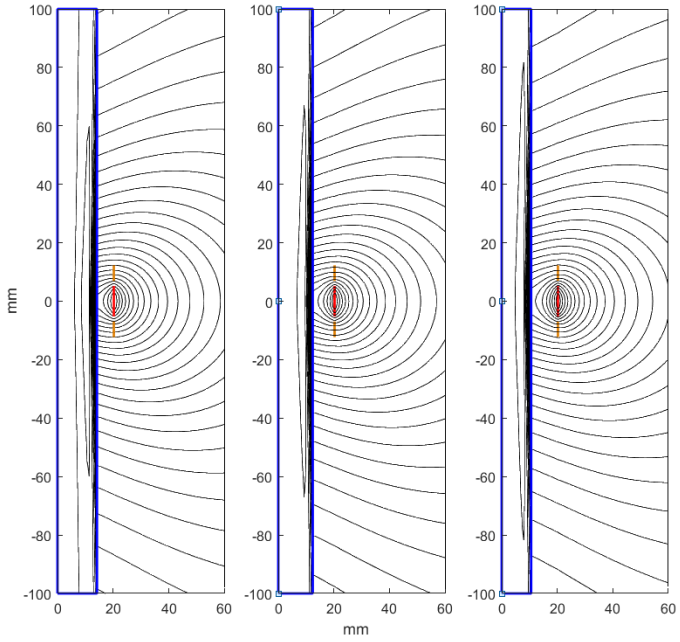

Fig. A2. Magnetic flux distribution at different positions of coils using analytical method, (left) equivalent iron rod radius = 14.2 mm, equivalent iron rod radius = 12.4 mm (middle), equivalent iron rod radius = 10.6 mm (right) - (f=100 Hz, $\mu_{r\text{-}i}$= 125)

APPENDIX B: ANNEALING PROCESS AND TEMPERATURE CURVE

The graph for annealing process is shown in Fig. B1, which was performed in MEDUNA vakuovakalirnas.ro (https://www.kalirna.cz). Two temperatures are shown, which one is for air temperature and second one is from temperature meter

inside of one sample located in close proximity to the conical iron rod.

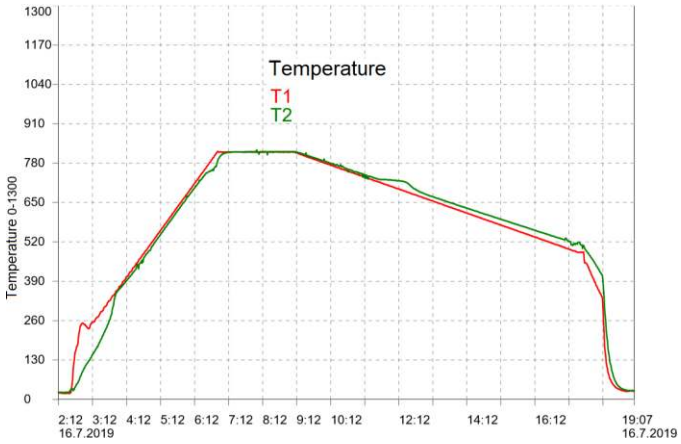

Fig. B1. Temperature profile of annealing process versus time (hour)

APPENDIX C: *B-H* CURVE AND MAGNETIC RELATIVE PERMEABILITY CURVE

Fig. C1 presents *B-H* curve and magnetic relative permeability curve of solid iron conical rod [28]. The initial relative magnetic permeability is extrapolated, which is estimated about 100 to 150 as direct measurement of B-H curve and relative magnetic permeability is problematic to measure

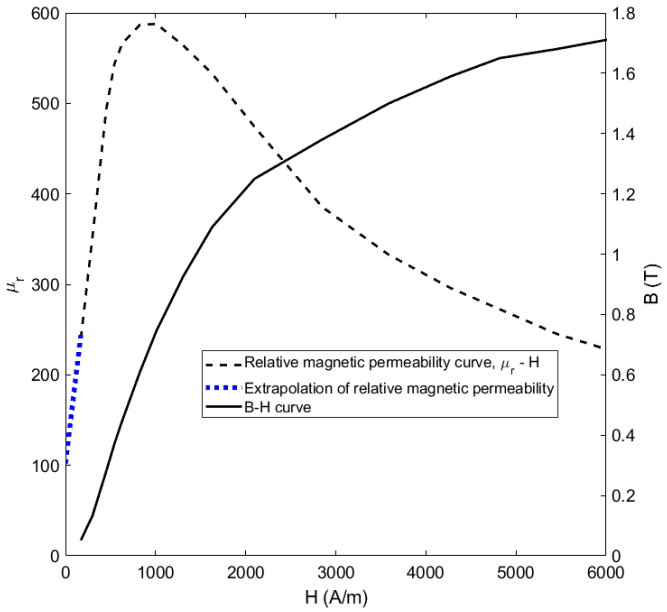

Fig. C1. *B-H* curve and relative magnetic permeability curve

REFERENCES

[1] S. C. Bera, R.Sarkar, M.Bhowmick, "Study of a modified differential inductance measurement circuit as position transducer of a power cylinder," *IEEE Trans. Instr. & Meas.*, vol. 61, no. 2, pp. 530-538, 2012

[2] P. Ripka, A. Chirtsov V. Grim, "Contactless piston position transducer with axial excitation," *IEEE Trans. Mag.*, vol. 53, no. 11, 2017, 4002504

[3] A. Kumar A. S., B. George, "A noncontact angle sensor based on eddy current technique," *IEEE Trans. Instr.& Meas.*, vol. 69, no. 4, pp. 1275-1283, 2020

[4] P. Ripka, *Magnetic Sensors and Magnetometers*, Artech House, Jan. 1,2001

[5] S. Fericean, A. Hiller-Brod, A. D. Dorneich, M. Fritton, "Microwave Displacement Sensor for Hydraulic Devices," *IEEE Sens. J.*, vol. 13, no. 12, 2013

[6] L. Shih-Yuan, L. Jyun, S. S. Lee, "The study of the piston driving and position sensing for a linearly moving piston pump," *Automatic Control Conference (CACS), 2014 CACS International, Kaohsiung*, 2014, pp. 287-291.

[7] K. Suzumori, J. Tanaka, T. Kanda, ""Development of an intelligent pneumatic cylinder and its application to pneumatic servo mechanism," *Proceedings, 2005 IEEE/ASME International Conference on Advanced Intelligent Mechatronics*., Monterey, CA, 2005, pp. 479-484.

[8] A. A. M. Faudzi, K. Suzumori, S. Wakimoto, "Design and control of new intelligent pneumatic cylinder for intelligent chair tool application," 2009 *IEEE/ASME International Conference on Advanced Intelligent Mechatronics*, Singapore, 2009, pp. 1909-1914.

[9] J. Vyhnanek, P.Ripka, A. Chirtsov, "Linear position sensing through conductive wall without permanent magnet," *Proc.* 2017, 1(4), 390

[10] H. Sumali, E.P. Bystrom, G.W. Krutz, "A displacement sensor for nonmetallic hydraulic cylinders," *IEEE Sens. J.*, vol. 3, no. 6, pp. 818 – 826, Dec. 2003

[11] B. Legrand, Y. Dordet, J. Y. Voyant, J.P. Yonnet, "Contactless position sensor using magnetic saturation," *Sens. & Act. A, Phys.*, vol. 106, no. 1–3, pp. 149–154, Sep. 2003

[12] P. Ripka, A. Chirtsov, M. Mirzaei, "Inductance position sensor for pneumatic cylinder," *AIP Advances*, 8, 2018, 048001

[13] M. Mirzaei, P. Ripka, A. Chirtsov, J. Vyhnanek, "Temperature influence on position transducer for pneumatic cylinder," *IEEE Sensors Conference 2018*, India paper #1638

[14] P. Ripka, M. Mirzaei, A. Chirtsov, J. Vyhnanek, "Transformer position sensor for a pneumatic cylinder," *Sens.& Act. A: Phys.*, 294, pp. 91–101, 2019

[15] Y. Kano, S. Hasebe, C. Huang, and T. Yamada, "New type linear variable differential transformer position transducer," *IEEE Trans. Instr.& Meas.,* vol. 38, no. 2, pp. 407 - 409, April 1989

[16] S. C. Saxena, S. B. L.Seksena, "A self-compensated smart LVDT transducer," *IEEE Trans. Instr.& Meas.,* 1989, 38, (3), pp. 748-753

[17] G .Y. Tian, Z.X. Zhao, R.W.Baines, N. Zhang, "Computational algorithms for linear variable differential transformers (LVDTs),"*IEE Proc.-Scie. Meas. Technol.*, vol. 144, no. 4, pp. 189-192, 1997

[18] S. K. Mishra, G. Panda, D. P. Das, "A novel method of extending the linearity range of linear variable differential transformer using artificial neural network,"*IEEE Trans. Instr. & Meas.*, vol. 59, no. 4, pp. 947-953, 2010

[19] S.-H. Yang, K. Hirata, T. Ota, and Y. Kawase, "Impedance linearity of contactless magnetic-type position sensor," *IEEE Trans. Mag.,* vol. 53, no. 6, pp. 1-4, June 2017

[20] J. F.Gieras, "Analytical method of calculating the electromagnetic field and power losses in ferromagnetic half space, taking into account saturation and hysteresis," *Proc. of the Inst. of Elec. Eng.*, vol. 124, no. 11, pp. 1098 -1104, 1977

[21] A. Sumner, C. Gerada, N. Brown, A. Clare, "Controlling DC permeability in cast steels," *J. of Mag.& Mag. Mat.,* vol. 429, pp. 79-85, 1 May 2017

[22] M. Lu, W. Zhu, L. Yin, A.J. Peyton, W. Yin, Z. Qu, "Reducing the lift-off effect on permeability measurement for magnetic plates from multi frequency induction data," *IEEE Trans. Instr. & Meas.*, vol. 67, no. 1, pp. 167 - 174, 2018

[23] P. Yang, M. Fan, B. Cao, S. Gao, "Investigation on Time-to-Peak Feature Insensitive to Liftoff Effect for Pulsed Eddy Current Evaluation," *IEEE Trans. Instr.& Meas.* 2019 (Early Access)

[24] A. Grima, M. D. Castro, A. Masi, N. Sammut, "Design enhancements of an ironless inductive position sensor," *IEEE Trans. Instr. & Meas.,* 2019 (Early access)

[25] B. Reinholz, R. J. Seethaler, "Design and validation of a variable reluctance differential solenoid transducer," *IEEE Sens. J.*, 2019 (Early access)

[26] K. J. Binns, P. J. Lawrenson, C. W. Trowbridge, *The Analytical and Numerical Solution of Electric and Magnetic Fields*, Wiley, 1 edition, December 1992

[27] M. Mirzaei, P. Ripka, A. Chirtsov, J. Vyhnanek, "Eddy current linear speed sensor," *IEEE Trans. Mag.*, vol. 55 , no. 1 , pp. 1-4, 2018

[28] M. Abramowitz and I. Stegun, *Handbook of Mathematical Functions with Formulas, Graphs, and Mathematical Tables*, National Bureau of Standards Applied Mathematics Series - 55, Ninth printing, 1970

[29] M. Mirzaei, P. Ripka, A. Chirtsov, J. Vyhnanek, "Impedance of iron conductors with circular and rectangular shapes," *IECON 2018 - 44th Annual Conference of the IEEE Industrial Electronics Society, Washington, DC, USA, 2018, pp. 194-199*

[30] D. O'Kelly, "Hysteresis and eddy-current losses in steel plates with nonlinear magnetisation characteristics," *Proc. of the Inst. of Elec. Eng.*, vol. 119, no. 11, pp. 1675 - 1676, 1972

[31] Y. Amara and G. Barakat, "Analytical modeling of magnetic field in surface mounted permanent-magnet tubular linear machines," *IEEE Trans. Mag.*, vol. 46 , no. 11 , pp. 3870-3884, 2010

[32] A. Musolino, R. Rizzo, and E. Tripodi, "Tubular linear induction machine as a fast actuator: Analysis and design criteria," *Prog. in Electromag. Research,* vol. 132, pp. 603–619, 2012

[33] A. D. Polyanin, *Handbook of Linear Partial Differential Equations for Engineers and Scientists*, Chapman & Hall/CRC, 2002

[34] ANSYS / Maxwell, Low Frequency Electromagnetic Field, V. 2019 R3, https://www.ansys.com/products/electronics/ansys-maxwell